

# Geophysical Research Letters



#### RESEARCH LETTER

10.1029/2024GL109062

#### **Key Points:**

- The formation of inverse temperature layer (ITL) is driven by strong solar radiation and moderate wind-driven turbulence
- The ITL depth has pronounced diurnal cycle shallower during daytime than during nighttime
- A physical model using observed solar radiation and water surface temperature captures the ITL dynamics

#### **Supporting Information:**

Supporting Information may be found in the online version of this article.

#### Correspondence to:

W. Jing, jasonjing@gatech.edu

#### Citation:

Jing, W., Wang, J., Liu, H., Shen, L., & Zhu, M. (2024). A mechanistic study of inverse temperature layer of water bodies. *Geophysical Research Letters*, 51, e2024GL109062. https://doi.org/10.1029/2024GL109062

Received 29 FEB 2024 Accepted 9 AUG 2024

#### **Author Contributions:**

Conceptualization: Weiqiang Jing,
Jingfeng Wang
Data curation: Weiqiang Jing,
Jingfeng Wang, Modi Zhu
Formal analysis: Weiqiang Jing
Funding acquisition: Jingfeng Wang,
Heping Liu, Lian Shen
Investigation: Jingfeng Wang
Methodology: Weiqiang Jing,
Jingfeng Wang
Project administration: Jingfeng Wang,
Heping Liu, Lian Shen
Resources: Jingfeng Wang
Supervision: Jingfeng Wang
Validation: Weiqiang Jing

© 2024. The Author(s).

This is an open access article under the terms of the Creative Commons

Attribution-NonCommercial-NoDerivs

License, which permits use and distribution in any medium, provided the original work is properly cited, the use is non-commercial and no modifications or adaptations are made.

Writing - original draft: Weiqiang Jing

Visualization: Weiqiang Jing

# A Mechanistic Study of Inverse Temperature Layer of Water Bodies

Weiqiang Jing<sup>1</sup>, Jingfeng Wang<sup>1</sup>, Heping Liu<sup>2</sup>, Lian Shen<sup>3</sup>, and Modi Zhu<sup>1</sup>

<sup>1</sup>Georgia Institute of Technology, Atlanta, GA, USA, <sup>2</sup>Washington State University, Pullman, WA, USA, <sup>3</sup>University of Minnesota, Minneapolis, MN, USA

**Abstract** The inverse temperature layer (ITL) beneath water-atmosphere interface within which temperature increases with depth has been observed from measurement of water temperature profile at an inland lake. Strong solar radiation combined with moderate wind-driven near-surface turbulence leads to the formation of a pronounced diurnal cycle of the ITL predicted by a physical heat transfer model. The ITL only forms during daytime when solar radiation intensity exceeds a threshold while consistently occurs during nighttime. The largest depth of the ITL is comparable to the *e*-fold penetration depth of solar radiation during daytime and at least one order of magnitude deeper during nighttime. The dynamics of the ITL depth variation simulated by a physical model forced by observed water surface solar radiation and temperature is confirmed by the observed water temperature profile in the lake.

**Plain Language Summary** An idealized one-dimensional heat transfer equation reveals the physical mechanisms of water temperature increasing with depth beneath the water-atmosphere interface known as inverse temperature layer (ITL). Solar radiation is the dominant forcing of water temperature profile while wind-driven turbulent mixing is a critical process determining whether the ITL forms. The limited depth of the ITL poses a constraint on the rate of heat transfer from the water body into the atmosphere. The dynamics of the ITL plays an important role in the water and energy cycle of large water bodies such as lakes and oceans.

#### 1. Introduction

Inverse temperature layer, in a boarder sense, is the part of a natural water body (e.g., lake, ocean, etc.) underneath the water-atmosphere interface where temperature increases with depth. The ITL is a ubiquitous phenomenon in the Earth system. The cool-skin on the top of oceans (Saunders, 1967; A. V. Soloviev & Schlüssel, 1994, 1996) is, for example, a thin (millimeter thick) conductive ITL. A recent observational study by J. Wang et al. (2023) reported a different type of ITL (referred to as the ITL herein) on the top of a large mid-latitude inland water body that differs from the cool-skin in several aspects. The concept of oceanic ITL was implied previously (A. Soloviev & Lukas, 2014) although direct field observations of oceanic ITL are not available, to our knowledge, but was hinted by circumstantial evidence (e.g., A. Soloviev & Lukas, 1997). Direct observation of the ITL is difficult as it requires high resolution (e.g.,  $\leq 10^{-1}$  m) measurements of water temperature profile beneath water-atmosphere interface. The ITL depth, defined as the distance below the water surface at which vertical temperature gradient vanishes (see Figure 1 of J. Wang et al. (2023)), was found to be on the order of 1 m with pronounced diurnal cycle, shallower during daytime and deeper during nighttime. The observations also revealed a close correspondence between the ITL structure (water temperature profile), solar radiation and water surface heat flux. The impact of wind speed on the ITL was evident but subtle. The ITL was found to persist through the seasons at a mid-latitude lake (J. Wang et al., 2023).

The ITL plays a critical role in the energy budget of water surface and exchange of water and heat between water bodies and the atmosphere, which are directly coupled with water temperature (J. Wang et al., 2023). The existence of the ITL is a necessary condition of heat transfer from water into the atmosphere. Solar radiation energy enters the water surface energy budget through heat transfer from warmer below-surface temperature toward cooler water surface through ITL without which only downward heat transfer at the water-atmosphere interface is possible. Contrary to the thin cool-skin with negligible thermal energy (heat) storage, the ITL has substantial heat storage resulting from the absorption of solar radiation. The change of the ITL heat storage is the only energy source of latent, sensible and outgoing longwave radiation flux at the surface when solar radiation is absent during

Writing – review & editing: Jingfeng Wang, Heping Liu, Lian Shen nighttime. The ITL dependent water surface heat flux (J. Wang et al., 2023) is a strong constraint on the latent and sensible heat flux over water surface.

Previous studies on the ITL indicate that it can vary between  $10^0$  and  $10^1$  m. The observed ITL has a clear diurnal cycle, being shallower during the day and deeper at night. Seasonal variations are also evident, with the ITL more pronounced in summer due to higher solar radiation (J. Wang et al., 2023). In this study, we investigate the mechanisms responsible for the observed behaviors of the ITL. Specially, we aim to identify the environmental conditions of the existence and diurnal cycle of the ITL focusing on the effect of solar radiation and wind driven near-surface turbulence on water temperature profile. A physical model of heat transfer of near-surface layer is used to characterize the combined effect of solar radiation and wind. An analytical solution of water temperature profile was derived to express the ITL depth, when exists, in terms of solar radiation intensity and wind speed dependent intensity of turbulence. The theoretically predicted and modeling analysis of the ITL is validated against available field observations of water temperature profile.

## 2. A Physical Model of the ITL

Temperature distribution of the water surface layer T(z, t) is often described by a one-dimensional heat transfer equation (Guo et al., 2021; Kirillin et al., 2021; Yang et al., 2017),

$$\frac{\partial T}{\partial t} = \frac{\partial}{\partial z} \left( \alpha \frac{\partial T}{\partial z} \right) + \frac{q_0(z, t)}{\rho_w c_w},\tag{1}$$

where  $z \ge 0$  is the water depth,  $\rho_w$  and  $c_w$  the density and specific heat of water, respectively,  $\alpha$  the eddy-diffusivity, and  $q_0$  represents the volume heat source due to the absorption of solar radiation by water. Horizontal advection is neglected when the size of the water body is much larger than the depth of water surface layer (Hostetler & Bartlein, 1990; Hostetler et al., 1994). Since the depth of the ITL is much smaller than that of water body (J. Wang et al., 2023), the depth of water body may be treated as semi-infinite (Gu et al., 2015; Karagounis et al., 1993; Subin et al., 2012). Use of a semi-infinite domain allows analytical solution of Equation 1 to facilitate the analysis of the ITL behavior.  $\alpha$ , characterizing water surface layer turbulence strongly affected by wind speed over the water surface, varies in principle with time and depth (Large et al., 1994; Van Roekel et al., 2018; Zhang et al., 2019). For the purpose of revealing the effect of water surface layer turbulence on the formation and diurnal cycle of the ITL, constant  $\alpha$  is assumed to characterize surface layer turbulence driven by fixed wind speed (with prescribed solar radiation heating). The representative values of  $\alpha$  may be obtained using a common parameterization (Henderson-Sellers, 1985).  $q_0$  is described by the Beer's Law (Defant, 1963; Hale & Querry, 1973),

$$q_0(z,t) = -\frac{\partial}{\partial z} \left\{ \exp\left(-\frac{z}{d}\right) \right\} R_n^s(t) \tag{2}$$

where d is the e-fold penetration depth of solar radiation and  $R_n^s$  the net solar radiation at water surface entering water body.

Equation 1 has an analytical solution in dimensionless form  $\tilde{T}(\tilde{z},\tilde{t})$  (A. Soloviev & Lukas, 2014),

$$\tilde{T}(\tilde{z}, \tilde{t}) = \int_{0}^{\tilde{t}} \tilde{T}(0, \tau) d \left[ erf \left( \frac{\tilde{z}}{2\sqrt{\tilde{\alpha}(\tilde{t} - \tau)}} \right) \right] 
+ \frac{1}{2} \int_{0}^{\tilde{t}} e^{\tilde{\alpha}(\tilde{t} - \tau)} \left[ e^{-\tilde{z}} erfc \left( \sqrt{\tilde{\alpha}(\tilde{t} - \tau)} - \frac{\tilde{z}}{2\sqrt{\tilde{\alpha}(\tilde{t} - \tau)}} \right) \right] 
- e^{\tilde{z}} erfc \left( \sqrt{\tilde{\alpha}(\tilde{t} - \tau)} + \frac{\tilde{z}}{2\sqrt{\tilde{\alpha}(\tilde{t} - \tau)}} \right) \right] \tilde{R}(\tau) d\tau$$
(3)

JING ET AL. 2 of 11

where  $\tilde{T} \equiv (T-T_0)/\Delta T$ ,  $T_0$  a constant reference temperature (e.g., uniform initial water temperature),  $\Delta T$  is an arbitrary constant diurnal amplitude of water surface temperature,  $\tilde{z} = z/d$ ,  $\tilde{t} = \omega_0 t$ ,  $\omega_0 \equiv 2\pi/\tau_0$ ,  $\tau_0$  the time scale (e.g., the length of day for diurnal cycle or the length of year for seasonal cycle), *erf* and *erfc* the error and complementary error function, respectively. The dimensionless solar radiation  $\tilde{R}$  and eddy-diffusivity are defined, respectively, as,

$$\tilde{\alpha} \equiv \frac{\alpha}{\omega_0 d^2}, \, \tilde{R} \equiv \frac{R_n^s}{\rho_w c_w \omega_0 d\Delta T} \tag{4}$$

Note that the dimensional solution of T(z, t) according to Equation 3 does not explicitly depend on  $\Delta T$  as both T(z, t) and  $R_n^s$  are non-dimensionalized by  $\Delta T$ , nor does it explicitly depends on  $\omega_0$  as both  $\alpha$  and t are non-dimensionalized by  $\omega_0$ . The analytical solution in Equation 3 is applicable to any time scale. The assumption of uniform initial water temperature as a mathematical convenience (for deriving the analytical solution) does not affect the usefulness of the analytical solution as long as the integration time is sufficient long (e.g., several days). An analytical solution of Equation 1 for the case of time-varying eddy-diffusivity  $\alpha(t)$  to represent the effect of variable wind speed is given in Equation A1 in Appendix A.

If the ITL forms, its depth is the shortest distance from the water surface  $\tilde{z}_0$  where water temperature reaches maximum solved from,

$$\frac{\partial \tilde{T}}{\partial \tilde{z}} = 0, \ \frac{\partial^2 \tilde{T}}{\partial \tilde{z}^2} < 0, \tag{5}$$

according to the analytical solution  $\tilde{T}$  in Equation 3.

## 3. Formation and Diurnal Cycle of the ITL

To reveal the role of net solar radiation in the formation and diurnal cycle of the ITL, an idealized diurnal cycle of solar radiation  $R_n^s$  is used in Equation 3 to simulate  $\tilde{T}(\tilde{z}, \tilde{t})$ ,

$$R_n^s = \max(R_0 \sin(\omega_0 t), 0) \tag{6}$$

where  $R_0$  is the constant diurnal amplitude of  $R_n^s$  and t = 0 is the local sunrise time. The effect of the heat exchange at the water-atmosphere interface on the formation and diurnal cycle of the ITL is characterized by an idealized water surface temperature,

$$T(0,t) = T_0 + \Delta T \sin(\omega_0 t + \phi_0) \tag{7}$$

where  $\Delta T$  is a constant diurnal amplitude of water surface temperature variations and  $\phi_0$  the constant phase difference between surface temperature and solar radiation. Field observations indicate  $\phi_0 \sim \pi/4$  (Yang et al., 2017). The effect of wind speed on the water surface energy budget is implicitly represented by the prescribed  $\Delta T$  (e.g.,  $\sim 1-3$ °C) as wind speed plays a crucial role in both atmosphere and water surface layer turbulence. Assumed constant  $\Delta T$ , like the constant eddy-diffusivity  $\alpha$  in Equation 1 and solar radiation  $R_0$  in Equation 6, facilitates the analysis of the mechanisms of the formation and diurnal cycle of the ITL.

Figure 1 shows the diurnal cycle of the (dimensionless) ITL depth  $\tilde{z}_0$  corresponding to the prescribed  $R_n^s$  and T(0,t) in Equations 6 and 7 varying with  $\tilde{\alpha}$  in Equation 4 and  $\Delta \tilde{R}$  defined as,

$$\Delta \tilde{R} \equiv \frac{\Delta R}{\rho_w c_w \omega_0 d\Delta T},\tag{8}$$

the sunrise time t=0 in Equation 6 is set as 6:00 in Figure 1. The white regions in the five panels of 08:00–16:00 indicate that the daytime ITL does not exist for certain combinations of  $\tilde{\alpha}$  and  $\Delta \tilde{R}$  when solar radiation intensity is low, for example,  $\Delta \tilde{R} < \sim 5$ , or  $\tilde{\alpha}$  is not too large depending on  $\Delta \tilde{R}$  when  $\Delta \tilde{R} > \sim 5$ . The ITL forms during

JING ET AL. 3 of 11

onlinelibrary.wiley.com/doi/10.1029/2024GL109062 by Jingfeng Wang - Georgia Institute Of Technology , Wiley Online Library on [27/08/2024]. See the Terms

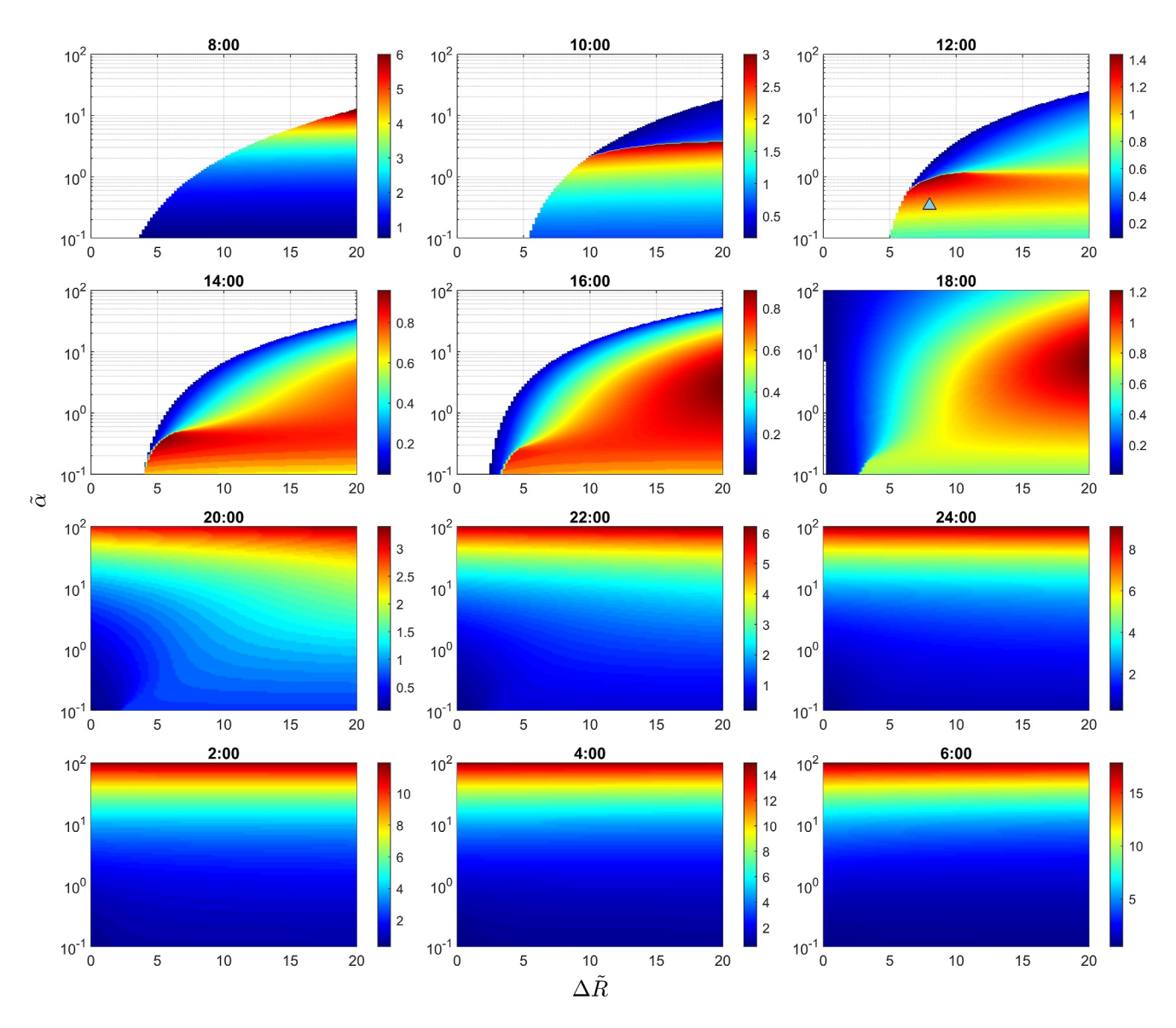


**Figure 1.** Diurnal cycle of the dimensionless inverse temperature layer depth  $\tilde{z}_0$  varying with  $\tilde{\alpha}$  in Equation 4 and  $\Delta \tilde{R}$  in Equation 8 derived from the analytical solution  $\tilde{T}$  in Equation 3. The blue triangle represents the value of  $\tilde{\alpha}$  and  $\Delta \tilde{R}$  from the observation.

daytime only when solar radiation is sufficiently strong while wind-driven turbulence is not too strong. Figure 1 further reveals that the daytime ITL reaches maximum at moderate  $\tilde{\alpha}$  (or wind speed). On the contrary, the ITL persists during nighttime regardless of the solar radiation intensity during daytime. The ITL depth during nighttime increases with  $\tilde{\alpha}$  (or wind speed) as shown in Figure 1.

It is important to emphasize that a shallower daytime ITL (Figure 1) does not necessarily correspond to a stronger temperature gradient near the water surface since wind-driven turbulent mixing tends to reduce the ITL temperature gradient. A greater  $\Delta \tilde{R}$  leads to a greater temperature gradient at the water surface everything else being equal. Large  $\tilde{\alpha}$  due to high wind speed may disrupt the ITL. Therefore, the ITL tends to form under the condition of strong solar radiation and moderate wind speed (or near-surface layer turbulence) as shown in Figure 1. Furthermore, Figure 1 shows a rapid decrease of the ITL depth around the sunrise time (more clearly demonstrated in Figure 2), suggesting the dominant role of solar radiation in the diurnal cycle of the ITL. This finding is confirmed by the observed and simulated ITL depth using observed solar radiation and water surface temperature (Figure 2) discussed next.

JING ET AL. 4 of 11

com/doi/10.1029/2024GL109062 by Jingfeng Wang - Georgia Institute Of Technology

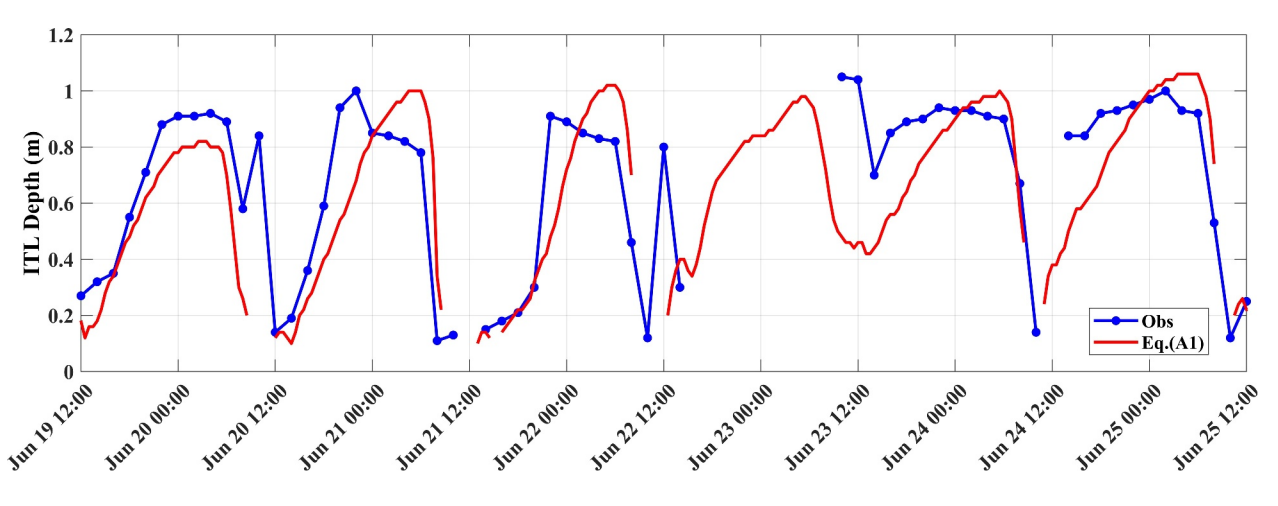


**Figure 2.** Observed (blue) versus simulated (red) inverse temperature layer depth using Equation A1 with observed solar radiation and water surface temperature for 19–25 June 2022

## 4. A Case Study

The theoretical analysis of the ITL shown in Figure 1 can be validated through modeling water temperature profile using Equation A1 forced by observed solar radiation, water surface temperature and wind speed for parameterizing eddy-diffusivity  $\alpha$  in Equation 1. The field observations were made at Ross Barnett Reservoir in Mississippi (32°26'N, 90°02'W) (Figure S1 in Supporting Information S1) (Liu et al., 2012). The observed solar radiation, water surface temperature and wind speed for 19-25 June 2022 used in this study are shown in Figure 3. Thermistors were installed at 0.05, 0.10, 0.15, 0.20, 0.25, 0.275, 0.35, 0.425, 0.5, 0.575, 0.825, 1.075, 1.325, 1.575 m depth at 1 min interval (model 107-L, Campbell Scientific, Inc.). Water temperature measured at 0.15, 0.20, and 1.575 m was excluded in this study due to sensor failure. During the study period, all sensors were recalibrated to correct biases using water surface temperature measured by an infrared thermometer. Since nocturnal mixing often causes nearly uniform temperature profile around midnight when wind speed exceeds 5 m s<sup>-1</sup> (Liu et al., 2016), all thermistors were re-calibrated by adding an offset relative to surface temperature. Due to limited resolution of water temperature measurements, the data points are interpolated to obtain a smooth temperature profile (see Supporting Information S1) for calculating the ITL depth according to Equation 5. Stronger nighttime mechanical mixing resulting from high wind speed leads to weak temperature gradient especially at deeper depth where the temperature data have lower resolution, making it difficult to derive the ITL depth from the interpolated smooth temperature profile. Those ITL depths were treated as missing points in Figure 2.

Numerous parameterizations of eddy diffusivity have been formulated in terms of wind speed, stratification, turbulent kinetic energy and dissipation rate. The commonly used Henderson-Sellers (1984) parameterization integrates the effects of forced and free convection on near-surface layer turbulence. The surface friction velocity expressed as a function of wind speed at 2 m is linked to the buoyancy frequency due to water density stratification. Another commonly used K-Profile Parameterization (Large et al., 1994; Van Roekel et al., 2018) of the eddy diffusivity is expressed in terms of a velocity scale and a vertical shape function. Buoyancy driven heat transfer caused by density gradient and wind shear (Large & Pond, 1982) is formulated based on Monin-Obukhov similarity theory (MOST) (Monin & Obukhov, 1954) in terms of a dimensionless similarity function of bulk Richardson number (Large et al., 1994). The similarity function may be approximated by, for example, a cubic polynomial with empirical coefficients (O'Brien, 1970). Eddy diffusivity may also be parameterized in terms of the dissipation rate of turbulent kinetic energy, often expressed in terms of density gradient dependent buoyancy frequency (Thorpe & Deacon, 1977). Alternatively, the dissipation rate can be expressed as a function of the kinetic energy flux into the mixed layer and the mixed-layer depth (Imberger, 1985). These formulas of eddy diffusivity have nearly uniform distribution across the near-surface layer (Colman & Armstrong, 1987; MacIntyre et al., 2021; Salas de Leon et al., 2016; Sweers, 1970; Y. Wang et al., 2019; Webster & Hutchinson, 1994; Zhang et al., 2019). Such formulated eddy diffusivity is shown to be useful only when averaged over the size of an

JING ET AL. 5 of 11

 $R_n^s (W m^{-2})$ 

Wind speed (m/s)

34

Jun 20 12:00

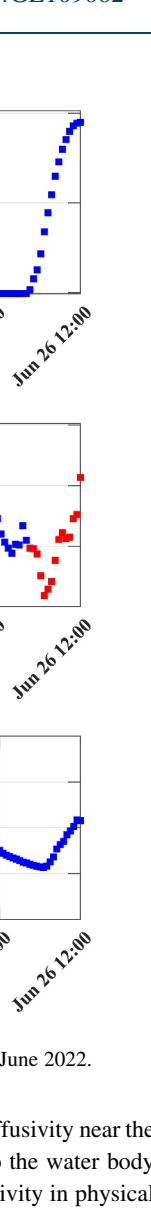


Figure 3. (a) Net solar radiation, (b) wind speed (daytime in red, nighttime in blue), (c) water surface temperature at Ross Barnett Reservoir 19-25 June 2022.

overturn (Thorpe & Deacon, 1977). Recent field measurements suggest a depth-uniform eddy diffusivity near the water surface (van Haren, 2019), especially for the case when the ITL is shallow compared to the water body depth (e.g., <~1 m vs. ~5-6 m (J. Wang et al., 2023)). The use of a depth-uniform eddy diffusivity in physical models has also been justified in previous studies (Boufadel et al., 2020; French-McCay et al., 2018; Paris et al., 2012). Time-dependent models align more closely with observed temporal dynamics of wind and solar radiation, making them practical and accurate for applications where spatial variations may not be as critical (Li et al., 2021). These models simplify the computational framework by focusing on temporal changes, reducing complexity and computational load compared to models accounting for both time and spatial variations, which is particularly beneficial in simulations where computational resources are limited (Holtslag & Moeng, 1991). Investigations into nonlinear heat equations have used time-dependent coefficients to better capture transient behaviors (Minh et al., 2018), acknowledging that turbulent transfer is significantly influenced by temporal changes in turbulence intensity (Vallis, 2017). Additionally, time-dependent models often require fewer parameters to define eddy diffusivity, making them easier to calibrate and adjust based on available data, which is particularly useful in scenarios where data on spatial variations are scarce or unreliable (Hanjalić & Launder, 2020). In this study, wind speed dependent formula of eddy diffusivity is used following Henderson-Sellers (1985) and Walters et al. (1978). The coefficient of eddy diffusivity formula (i.e.,  $6.5 \times 10^{-6}$ ) in Equation A3 in Appendix A estimated from the observed water temperature profile is consistent with a recent study of a shallow lake (van Haren, 2019). A detailed comparison can be found in Supporting Information S1.

The physical model captures the diurnal cycle of the ITL depth (Figure 2) with the simulated temperature profile (Figure S2 in Supporting Information S1). Daytime ITL depth  $\sim$ 0.1 m is consistent with the observed ITL depth derived from the measured water temperature profile. The modeled ITL depth is shallower during daytime and

JING ET AL. 6 of 11

growing quickly deeper around the sunset time reaching its maximum around sunrise time next day. During the study period,  $\Delta \tilde{R} \sim 8$  with the measured e-fold penetration depth  $d \sim 0.3$  m and  $\Delta T \simeq 1.4$  °C at the Ross Barnett Reservoir. The representative eddy-diffusivity  $\alpha \simeq 10^{-6}$  m<sup>2</sup> s<sup>-1</sup> under daytime moderate wind and more stable condition (Figure S3 in Supporting Information S1) (Vercauteren et al., 2011) corresponds to  $\tilde{\alpha} \simeq 0.34$ . The persistent ITL during the study period is confirmed by the observed dimensionless parameters  $\tilde{\alpha}$  and  $\Delta \tilde{R}$  located within the domain of the formation of the ITL (Figure 1).

The discrepancies between the observed and modeled ITL depth (Figure 2) arguably have two main causes. First, the expression in Equation A3 in Appendix A assumes a linear relationship between eddy diffusivity and wind speed with a constant coefficient. While using a wind speed dependent formula of eddy diffusivity has been justified, linear dependence of eddy diffusivity on wind speed may be less accurate than other formulas (e.g., power function as Equation 22 in Henderson-Sellers (1985)) since it may over- or underestimate the simulated water temperature profile and the ITL depth. Eddy diffusivity expressed in the form of a nonlinear function of wind speed may improve the model simulations. However, the estimation of multiple parameters of nonlinear empirical formula is subject to the over-fitting problem (Vercauteren et al., 2011). Second, re-calibration of below-surface thermistors against infrared thermometer may not correct all systematic biases. Limited spatial resolution of temperature data and missing data points due to sensor failure during the study period lead to more measurement errors of temperature profile, hence higher uncertainty of the derived ITL depth. This is particularly of concern during nighttime when deeper ITL depth (than during daytime) is located where the spacing between thermistors is greater. Despite of the measurement errors of the temperature profile, the reasonable agreement between the observed ITL depth and the model simulations in Figure 2 indicates that the idealized physical model is able to capture the main features of the ITL dynamics at diurnal scale.

## 5. Turbulence in the Lake Surface Layer With the Existence of ITL

The analysis of the ITL's impact on surface layer turbulence uses the data from 2007, which includes lake temperature profiles down to 4.5 m below the surface. Recently, to better capture ITL dynamics near the surface, temperature sensors were repositioned closer to the lake surface, resulting in a lack of temperature profiles for deeper layers. Detailed information about the previous experimental setup is available in studies by J. Wang et al. (2023) and Liu et al. (2012). Diurnal stratification and mixing in the upper water column of Ross Barnett Reservoir are directly linked to surface buoyancy flux  $\beta$ , and friction velocity  $u_*$ .  $\beta$  is calculated as  $\beta = g\alpha H/(C_p\rho_s)$ , where g is gravity,  $\alpha$  is the thermal coefficient of expansion, H is lake surface heat flux,  $C_p$  is specific heat capacity, and  $\rho_s$  is the density of water at the surface. During the morning heating period with low to moderate wind speed around 1 m s<sup>-1</sup>, as on 28 and 29 August, low  $u_*^3$  minimally drives near-surface mechanical mixing (Figure 4b), the water below the lake surface heats rapidly, causing the depth of the ITL to become shallower (Figure 4c). A diurnal thermocline develops, separating the actively mixing layer from the remnant layer. With the presence of the ITL, surface buoyancy flux is always negative, indicating an inverse density gradient (density decreasing with depth). Convective mixing of the ITL is enhanced as the magnitude of  $\beta$  increases due to the shallower daytime ITL(~0.3 m), accompanied by the descent of the diurnal thermocline (Figure 4c). Shallower daytime ITL could disrupt the ITL through enhanced convective mixing, but insufficient to destroy the ITL (Figure 4c).

The depth of the actively mixing layer  $z_{\rm AML}$  (Figure 4c) is determined from the lake temperature profile based on the criterion by MacIntyre et al. (2021). Strong daytime solar radiation with a peak of approximately 900 Wm<sup>-2</sup> at noontime results in positive effective heat flux  $H_*$  (the sum of surface heat flux H and solar radiation absorbed within the actively mixing layer  $z_{\rm AML}$ ) (Imberger, 1985). Buoyancy flux into the actively mixing layer  $\beta_*$  indicates heating or cooling within the actively mixing layer (calculated from  $H_*$  instead of H) (MacIntyre et al., 2021; Tedford et al., 2014), often increases to about  $4\times 10^{-7}~{\rm m}^{-2}~{\rm s}^{-3}$  at noontime (Figure 4a), indicating a strong solar heating within the actively mixing layer. The water friction velocity is  $u_{*w} = \sqrt{\frac{\tau}{\rho_w}}$  with  $\rho_w$  the density of water and  $\tau$  the shear stress on the lake surface assuming that shear stress is continuous at the air–water interface (MacIntyre et al., 2021; Ramón et al., 2022; Tedford et al., 2014). The Monin-Obukhov length of the water surface layer,  $L_{\rm MO} = u_{*w}^3/\kappa\beta_*$ , characterize the relative magnitude of turbulence production from wind and from buoyancy flux (Csanady, 2001). The ratio  $|L_{\rm MO}/z_{\rm AML}|$  represents the fraction of the surface layer in which shear production of turbulence dominates over buoyancy flux (Imberger, 1985).  $|L_{\rm MO}/z_{\rm AML}| > 1$  implies that

JING ET AL. 7 of 11

com/doi/10.1029/2024GL109062 by Jingfeng Wang - Georgia Institute Of Technology, Wiley Online Library on [27/08/2024]. See the Terms

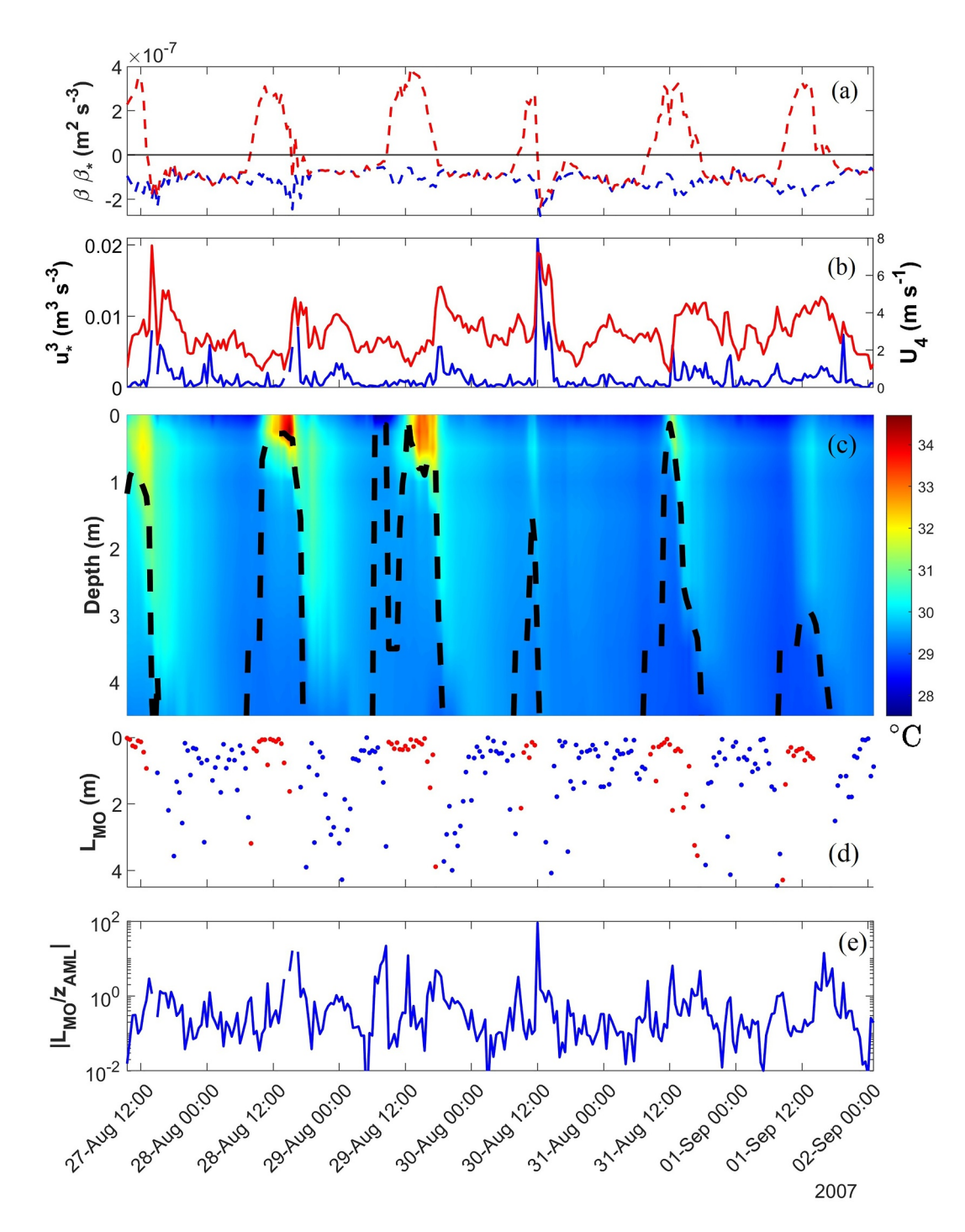


Figure 4. (a) Surface buoyancy flux ( $\beta$ ) (blue), and buoyancy flux into the actively mixing layer( $\beta_*$ ) (red), (b) Friction velocity cubed ( $u_*^3$ ) (blue) and wind speed at 4 m ( $U_4$ ) (red), (c) Temperature profile with actively mixing layer depth ( $z_{\rm AML}$ ) (black dashed), (d) Monin-Obukhov length scale ( $L_{\rm MO}$ ) in the water under heating (red) and cooling (blue) (e)  $|L_{\rm MO}/z_{\rm AML}|$  at Ross Barnett Reservoir 27 August–02 September 2007.

wind dominates turbulence production in the actively mixing layer (MacIntyre et al., 2021). During the daytime heating period with low and moderate wind and large  $\beta_*$ , for example, 28 and 29 August,  $L_{\rm MO}$  approaches zero, corresponding to strong near-surface stratification. Near sunrise, following nocturnal cooling and stronger wind,  $z_{\rm AML}$  is at the top of the seasonal thermocline (Tedford et al., 2014). On windier days such as 30 August and 1 September,  $L_{\rm MO}$  often extends beyond  $z_{\rm AML}$ , indicating strong wind shear predominantly drives turbulence

JING ET AL. 8 of 11

throughout most of the mixing layer. Observations indicate that wind-induced mechanical mixing is stronger than thermally induced convection in disrupting the ITL (Figures 4c and 4e).

#### 6. Conclusion

Solar radiation and wind-driven surface layer turbulence are shown to be the dominant mechanisms of the formation and diurnal cycle of the ITL. The daytime ITL only occurs when solar radiation intensity is sufficiently strong and wind-driven surface layer turbulent mixing is moderate. Strong wind tends to destroy the ITL even for strong solar radiation. The ITL prevails during the night regardless of the daytime solar radiation intensity and wind speed. The ITL depth has pronounced diurnal cycle shallower during daytime and deeper during nighttime. The daytime ITL depth is comparable to the e-fold penetration depth of solar radiation. For a given level of solar radiation intensity, maximum ITL depth corresponds to an intermediate wind speed. The ITL depth is at least one order of magnitude greater during nighttime than daytime. The behavior of the ITL predicted by the physical model is confirmed by field observations at an inland lake.

#### Appendix A: Analytical Solution of Equation 1 with Variable $\alpha$

The analytical solution of Equation 1 with variable eddy-diffusivity  $\alpha(t)$  is expressed,

$$T(z,t) = \int_{0}^{t} T(0,\tau) d \left[ erf\left(\frac{z}{2\sqrt{D(t,\tau)}}\right) \right]$$

$$+ \frac{1}{2\rho_{w}c_{w}d} \int_{0}^{t} exp\left(-\frac{D(t,\tau)}{d^{2}}\right) \left[ exp\left(-\frac{z}{d}\right) erfc\left(\frac{\sqrt{D(t,\tau)}}{d} - \frac{z}{2\sqrt{D(t,\tau)}}\right) \right]$$

$$- exp\left(\frac{z}{d}\right) erfc\left(\frac{\sqrt{D(t,\tau)}}{d} + \frac{z}{2\sqrt{D(t,\tau)}}\right) \right] R_{n}^{s}(\tau) d\tau$$

$$+ \frac{1}{2} \int_{0}^{\infty} T(\xi,0) d \left[ erf\left(\frac{\xi - z}{2\sqrt{D(t,0)}}\right) - erf\left(\frac{\xi + z}{2\sqrt{D(t,0)}}\right) \right]$$
(A1)

where  $\tau$  and  $\xi$  are integration (time and depth) variables, respectively, and

$$D(t,\tau) = \int_{-\tau}^{t} \alpha(s)ds \tag{A2}$$

A derivation of Equation 9 is given in Supporting Information S1. The lake surface temperature T(0, t) may be solved from coupled water and surface atmospheric models (Jing & Wang, 2023; Kayastha et al., 2023; MacKay, 2012).

The eddy diffusivity is parameterized by 2 m wind speed U (Henderson-Sellers, 1985), given by

$$\alpha = 6.5 \times 10^{-6} U. \tag{A3}$$

#### **Data Availability Statement**

The data used in this study is publicly available from Jing (2024) and J. Wang et al. (2022).

### References

Boufadel, M., Liu, R., Zhao, L., Lu, Y., Özgökmen, T., Nedwed, T., & Lee, K. (2020). Transport of oil droplets in the upper ocean: Impact of the eddy diffusivity. *Journal of Geophysical Research: Oceans*, 125(2), e2019JC015727. https://doi.org/10.1029/2019JC015727

Colman, J. A., & Armstrong, D. E. (1987). Vertical eddy diffusivity determined with <sup>222</sup>Rn in the benthic boundary layer of ice-covered lakes. Limnology and Oceanography, 32(3), 577–590. https://doi.org/10.4319/lo.1987.32.3.0577

Csanady, G. (2001). Air-sea interaction: Laws and mechanisms. Cambridge University Press.

Defant, A. (1963). Physical oceanography. Annales de Géographie, 72(390), 195–196. https://doi.org/10.3406/geo.1963.16378

French-McCay, D. P., Tajalli-Bakhsh, T., Jayko, K., Spaulding, M. L., & Li, Z. (2018). Validation of oil spill transport and fate modeling in Arctic ice. Arctic Science, 4(1), 71–97. https://doi.org/10.1139/as-2017-0027

Meteorology Program Grants EAR-2006281 (Georgia Institute of Technology), EAR-2002644 (Washington State University), and EAR-2003076

National Science Foundation Hydrological

This study is jointly sponsored by the

Sciences and Physical and Dynamic

(University of Minnesota).

JING ET AL.

Acknowledgments

\_\_\_\_\_

9 of 11



## **Geophysical Research Letters**

- 10.1029/2024GL109062
- Gu, H., Jin, J., Wu, Y., Ek, M. B., & Subin, Z. M. (2015). Calibration and validation of lake surface temperature simulations with the coupled WRF-lake model. *Climatic Change*, 129(3–4), 471–483. https://doi.org/10.1007/s10584-013-0978-y
- Guo, M., Zhuang, Q., Yao, H., Golub, M., Leung, L. R., Pierson, D., & Tan, Z. (2021). Validation and sensitivity analysis of a 1D lake model across global lakes. *Journal of Geophysical Research: Atmospheres*, 126(4), e2020JD033417. https://doi.org/10.1029/2020JD033417
- Hale, G. M., & Querry, M. R. (1973). Optical constants of water in the 200-nm to 200-μm wavelength region. Applied Optics, 12(3), 555–563. https://doi.org/10.1364/AO.12.000555
- Hanjalić, K., & Launder, B. E. (2020). Eddy-viscosity transport modelling: A historical review. In A. Runchal (Ed.), 50 years of CFD in engineering sciences: A commemorative volume in memory of D. Brian spalding (pp. 295–316). Springer Singapore. https://doi.org/10.1007/978-981-15-2670-1
- Henderson-Sellers, B. (1984). Development and application of "U.S.E.D.": A hydroclimate lake stratification model. *Ecological Modelling*, 21(4), 233–246. https://doi.org/10.1016/0304-3800(84)90061-9
- Henderson-Sellers, B. (1985). New formulation of eddy diffusion thermocline models. Applied Mathematical Modelling, 9(6), 441–446. https://doi.org/10.1016/0307-904X(85)90110-6
- Holtslag, A. A. M., & Moeng, C.-H. (1991). Eddy diffusivity and countergradient transport in the convective atmospheric boundary layer. *Journal of the Atmospheric Sciences*, 48(14), 1690–1698. https://doi.org/10.1175/1520-0469(1991)048\(1690:EDACTI\)2.0.CO;2
- Hostetler, S. W., & Bartlein, P. J. (1990). Simulation of lake evaporation with application to modeling lake level variations of Harney-Malheur Lake, Oregon. Water Resources Research, 26(10), 2603–2612. https://doi.org/10.1029/WR026i010p02603
- Hostetler, S. W., Giorgi, F., Bates, G. T., & Bartlein, P. J. (1994). Lake-atmosphere feedbacks associated with paleolakes Bonneville and Lahontan. *Science*, 263(5147), 665–668. https://doi.org/10.1126/science.263.5147.665
- Imberger, J. (1985). The diurnal mixed layer. Limnology and Oceanography, 30(4), 737-770. https://doi.org/10.4319/lo.1985.30.4.0737
- Jing, W. (2024). A mechanistic study of inverse temperature layer of water bodies [Dataset]. Zenodo. https://doi.org/10.5281/zenodo.10725695 Jing, W., & Wang, J. (2023). A dynamics of surface temperature forced by solar radiation. Geophysical Research Letters, 50(3), e2022GL101222. https://doi.org/10.1029/2022GL101222
- Karagounis, I., Trösch, J., & Zamboni, F. (1993). A coupled physical-biochemical lake model for forecasting water quality. Aquatic Science, 55(2), 87–102. https://doi.org/10.1007/BF00877438
- Kayastha, M. B., Huang, C., Wang, J., Pringle, W. J., Chakraborty, T., Yang, Z., et al. (2023). Insights on simulating summer warming of the Great Lakes: Understanding the behavior of a newly developed coupled lake-atmosphere modeling system. *Journal of Advances in Modeling Earth Systems*, 15(7), e2023MS003620. https://doi.org/10.1029/2023MS003620
- Kirillin, G. B., Shatwell, T., & Wen, L. (2021). Ice-covered lakes of Tibetan Plateau as solar heat collectors. *Geophysical Research Letters*, 48(14), e2021GL093429. https://doi.org/10.1029/2021GL093429
- Large, W. G., McWilliams, J. C., & Doney, S. C. (1994). Oceanic vertical mixing: A review and a model with a nonlocal boundary layer parameterization. Reviews of Geophysics, 32(4), 363–403. https://doi.org/10.1029/94RG01872
- Large, W. G., & Pond, S. (1982). Sensible and latent heat flux measurements over the ocean. *Journal of Physical Oceanography*, 12(5), 464–482. https://doi.org/10.1175/1520-0485(1982)012\(0464:SALHFM\)\(2.0.CO;\)2
- Li, Q., Cheng, Y., & Gentine, P. (2021). Connection between mass flux transport and eddy diffusivity in convective atmospheric boundary layers. Geophysical Research Letters, 48(8), e2020GL092073. https://doi.org/10.1029/2020gl092073
- Liu, H., Zhang, Q., & Dowler, G. (2012). Environmental controls on the surface energy budget over a large southern inland water in the United States: An analysis of one-year eddy covariance flux data. *Journal of Hydrometeorology*, *13*(6), 1893–1910. https://doi.org/10.1175/JHM-D-12.000.1
- Liu, H., Zhang, Q., Katul, G. G., Cole, J. J., Chapin, F. S., & MacIntyre, S. (2016). Large CO<sub>2</sub> effluxes at night and during synoptic weather events significantly contribute to CO<sub>2</sub> emissions from a reservoir. *Environmental Research Letters*, 11(6), 064001. https://doi.org/10.1088/1748-9326/
- MacIntyre, S., Amaral, J. H. F., & Melack, J. M. (2021). Enhanced turbulence in the upper mixed layer under light winds and heating: Implications for gas fluxes. *Journal of Geophysical Research: Oceans*, 126(12), e2020JC017026. https://doi.org/10.1029/2020JC017026
- MacKay, M. D. (2012). A process-oriented small lake scheme for coupled climate modeling applications. *Journal of Hydrometeorology*, 13(6), 1911–1924. https://doi.org/10.1175/jhm-d-11-0116.1
- Minh, T. L., Hong, P. L., & Hoang, Q. P. (2018). An asymmetric backward problem for the inhomogeneous parabolic equation with time-dependent diffusivity. Computational and Applied Mathematics, 37(3), 3241–3255. https://doi.org/10.1007/s40314-017-0509-y
- Monin, A. S., & Obukhov, A. M. (1954). Basic laws of turbulent mixing in the atmospheric near the ground. Akad. Naud. SSSR Geofiz. Inst., 24, 163–187.
- O'Brien, J. J. (1970). A note on the vertical structure of the eddy exchange coefficient in the planetary boundary layer. *Journal of the Atmospheric Sciences*, 27(8), 1213–1215. https://doi.org/10.1175/1520-0469(1970)027(1213:ANOTVS)2.0.CO;2
- Paris, C. B., Hénaff, M. L., Aman, Z. M., Subramaniam, A., Helgers, J., Wang, D.-P., et al. (2012). Evolution of the Macondo well blowout: Simulating the effects of the circulation and synthetic dispersants on the subsea oil transport. *Environmental Science & Technology*, 46(24), 13293–13302. https://doi.org/10.1021/es303197h
- Ramón, C. L., Ulloa, H. N., Doda, T., & Bouffard, D. (2022). Flushing the lake littoral region: The interaction of differential cooling and mild winds. Water Resources Research, 58(3), e2021WR030943. https://doi.org/10.1029/2021WR030943
- Salas de Leon, D., Alcocer, J., Ardiles, V., & Quiroz-Martínez, B. (2016). Estimation of the eddy diffusivity coefficient in a warm monomictic tropical lake. *Journal of Limnology*, 75(s1). https://doi.org/10.4081/jlimnol.2016.1431
- Saunders, P. M. (1967). The temperature at the ocean-air interface. *Journal of the Atmospheric Sciences*, 24(3), 269–273. https://doi.org/10.1175/1520-0469(1967)024(0269:TTATOA)2.0.CO;2
- Soloviev, A., & Lukas, R. (1997). Observation of large diurnal warming events in the near-surface layer of the western equatorial Pacific warm pool. *Deep Sea Research Part 1: Oceanographic Research Papers*, 44(6), 1055–1076. https://doi.org/10.1016/S0967-0637(96)00124-0
- Soloviev, A., & Lukas, R. (2014). The near-surface layer of the ocean (Vol. 48). Springer. https://doi.org/10.1007/978-94-007-7621-0
- Soloviev, A. V., & Schlüssel, P. (1994). Parameterization of the cool skin of the ocean and of the air-ocean gas transfer on the basis of modeling surface renewal. *Journal of Physical Oceanography*, 24(6), 1339–1346. https://doi.org/10.1175/1520-0485(1994)024(1339:POTCSO)2.0. CO;2
- Soloviev, A. V., & Schlüssel, P. (1996). Evolution of cool skin and direct air-sea gas transfer coefficient during daytime. *Boundary-Layer Meteorology*, 77(1), 45–68. https://doi.org/10.1007/BF00121858
- Subin, Z. M., Murphy, L. N., Li, F., Bonfils, C., & Riley, W. J. (2012). Boreal lakes moderate seasonal and diurnal temperature variation and perturb atmospheric circulation: Analyses in the community earth system model 1 (CESM1). *Tellus A: Dynamic Meteorology and Ocean-ography*, 64(1), 15639. https://doi.org/10.3402/tellusa.v64i0.15639

JING ET AL. 10 of 11

- Sweers, H. E. (1970). Vertical diffusivity coefficient in a thermocline. Limnology and Oceanography, 15(2), 273–280. https://doi.org/10.4319/lo. 1970 15 2 0273
- Tedford, E. W., MacIntyre, S., Miller, S. D., & Czikowsky, M. J. (2014). Similarity scaling of turbulence in a temperate lake during fall cooling. *Journal of Geophysical Research: Oceans*, 119(8), 4689–4713. https://doi.org/10.1002/2014JC010135
- Thorpe, S. A., & Deacon, G. E. R. (1977). Turbulence and mixing in a Scottish loch. Philosophical Transactions of the Royal Society of London. Series A, Mathematical and Physical Sciences, 286(1334), 125–181. https://doi.org/10.1098/rsta.1977.0112
- Vallis, G. K. (2017). Turbulent diffusion and eddy transport. In Atmospheric and oceanic fluid dynamics: Fundamentals and large-scale circulation (pp. 473–508). Cambridge University Press.
- van Haren, H. (2019). Turbulent convection and high-frequency internal wave details in 1-m shallow waters. *Limnology and Oceanography*, 64(3), 1323–1332. https://doi.org/10.1002/lno.11118
- Van Roekel, L., Adcroft, A. J., Danabasoglu, G., Griffies, S. M., Kauffman, B., Large, W., et al. (2018). The KPP boundary layer scheme for the ocean: Revisiting its formulation and benchmarking one-dimensional simulations relative to LES. *Journal of Advances in Modeling Earth Systems*, 10(11), 2647–2685. https://doi.org/10.1029/2018MS001336
- Vercauteren, N., Huwald, H., Bou-Zeid, E., Selker, J. S., Lemmin, U., Parlange, M. B., & Lunati, I. (2011). Evolution of superficial lake water temperature profile under diurnal radiative forcing. Water Resources Research, 47(9). https://doi.org/10.1029/2011WR010529
- Walters, R. A., Carey, G. F., & Winter, D. R. (1978). Temperature computation for temperate lakes. *Applied Mathematical Modelling*, 2(1), 41–48. https://doi.org/10.1016/0307-904x(78)90034-3
- Wang, J., Liu, H., & Shen, L. (2022). An observational and modeling study of inverse-temperature layer and water surface heat flux. [Dataset]. Zenodo. https://doi.org/10.5281/zenodo.7179025
- Wang, J., Liu, H., & Shen, L. (2023). An observational and modeling study of inverse-temperature layer and water surface heat flux. *Geophysical*
- $Research\ Letters, 50(16), e2023GL104358.\ https://doi.org/10.1029/2023GL104358$   $Wang,\ Y.,\ Ma,\ Q.,\ Gao,\ Y.,\ Hao,\ X.,\ \&\ Liu,\ S.\ (2019).\ Simulation\ of\ the\ surface\ energy\ flux\ and\ thermal\ stratification\ of\ lake\ Taihu\ with\ three\ 1-D$
- models. Water, 11(5), 1026. https://doi.org/10.3390/w11051026

  Webster, I. T., & Hutchinson, P. A. (1994). Effect of wind on the distribution of phytoplankton cells in lakes revisited. Limnology and
- Oceanography, 39(2), 365–373. https://doi.org/10.4319/lo.1994.39.2.0365
- Yang, J., Wang, Z.-H., Li, Q., Vercauteren, N., Bou-Zeid, E., & Parlange, M. B. (2017). A novel approach for unraveling the energy balance of water surfaces with a single depth temperature measurement. *Limnology and Oceanography*, 62(1), 89–103. https://doi.org/10.1002/lno.10378
- Zhang, Q., Jin, J., Wang, X., Budy, P., Barrett, N., & Null, S. E. (2019). Improving lake mixing process simulations in the community land model by using k profile parameterization. Hydrology and Earth System Sciences, 23(12), 4969–4982. https://doi.org/10.5194/hess-23-4969-2019

## **References From the Supporting Information**

- Doyle, T., Commission, U. A. E., & Laboratory, L. A. S. (1973). Nonlinear least squares optimization of a continuous n-parameter system. Los Alamos Scientific Laboratory of the University of California. Retrieved from https://books.google.com/books?id=f7eZmqmuLkC
- Gregg, M., D'Asaro, E., Riley, J., & Kunze, E. (2018). Mixing efficiency in the ocean. Annual Review of Marine Science, 10(1), 443–473. https://doi.org/10.1146/10.1146/annurev-marine-121916-063643
- Oakey, N. S. (1982). Determination of the rate of dissipation of turbulent energy from simultaneous temperature and velocity shear microstructure measurements. *Journal of Physical Oceanography*, 12(3), 256–271. https://doi.org/10.1175/1520-0485(1982)012(0256:DOTROD)2.0.CO;2
- Osborn, T. R. (1980). Estimates of the local rate of vertical diffusion from dissipation measurements. *Journal of Physical Oceanography*, 10(1), 83–89. https://doi.org/10.1175/1520-0485(1980)010(0083;EOTLRO)2.0.CO;2
- Yuan, Y.-X. (2000). A review of trust region algorithms for optimization. In ICIAM (Vol. 99, pp. 271–282). https://doi.org/10.1093/oso/9780198505143.003.0023

JING ET AL. 11 of 11